Integrating Circuit Level Simulation and Monte-Carlo Radiation Transport Code for Single Event Upset Analysis in SEU Hardened Circuitry

Kevin M. Warren, Andrew L. Sternberg, Robert A. Weller, Mark P. Baze, Lloyd W. Massengill, Robert A. Reed, Marcus H. Mendenhall, and Ronald D. Schrimpf

***Abstract*—Monte-Carlo radiation transport code is coupled with SPICE circuit level simulation to identify regions of single event upset vulnerability in an SEU hardened flip-flop, as well as predict single event upset cross sections and on-orbit soft error rates under static and dynamic operating conditions.**

***Index Terms*—Geant4, MRED, rate prediction, SEU, SPICE.**

I. Introduction

In this work, a new approach for analyzing single-event effects in circuits is proposed. The methodology allows for calibration of simulation parameters to accelerator beam data by high-fidelity radiation transport and energy deposition calculation of particles in a user-definable environment where circuit level simulation of each energy deposition event is performed. The goal is achieved by using Monte-Carlo Energy Deposition software (MRED) directly coupled with SPICE. The software is used to analyze the SEU characteristics of a dual interlocked cell (DICE) radiation hardened flip-flop containing 64 transistors.

The technique provides an immediate measure of the single event response as it pertains to the relationship between cross sections, layout and circuit response. Simulation results identify vulnerabilities in circuit design and layout to SEU and the predicted cross sections are in good agreement with experimental data. Limitations and systematic uncertainty in the modeling approach as well as the impact of limited heavy ion cross sectional data are discussed.

Monte-Carlo radiation transport codes such as Geant4 [1]–[4] and those using the Geant4 libraries such as MRED [5]–[12] and the Geant4 Microdosimetry Analysis tool (GMAT) [13] have been used extensively in single event upset (SEU) analyses for integrated circuits. Proprietary code has also been developed to perform similar analysis [14]. In [12] and [14], [15], radiation transport software was coupled directly with technology computer aided design (TCAD) solvers to predict transistor and circuit level response in problems that required consideration of nuclear reactions and the trajectories of the resultant products. In [14], the authors describe using the resulting TCAD output as input for circuit simulations to evaluate valid error conditions at the circuit level. Physics based simulators have been used to calculate error rates for static random access memories (SRAM) [5]–[9], dynamic random access memories (DRAM) [2], and recently for more complicated circuits such as single stage radiation hardened by design (RHBD) latches [11].

In [5], [10], and [15] various radiation transport codes were used to evaluate historical heavy ion test methods and provide insight into experimental observations of the interaction of back end of line (BEOL) materials with high energy ions and the effects of ion energy on SEU cross sections.

Geant4 was presented as an alternative to classical analytical SEU rate predictions methods in [16]. A similar technique was developed for use in MRED, which was first presented as a solution for quantifying on-orbit SEU rates in SRAM devices [17]. It was found that nuclear reactions from galactic cosmic rays passing through the BEOL materials dominated the on-orbit SEU rate. The use of physics based code, which contains models for nuclear fragmentation, were required to predict the SEU rate accurately. Classical approaches under-predicted the on-orbit rate by two orders of magnitude.

Monte-Carlo radiation transport codes, including coupling to external software packages, are thus well established as a means for determining SEU cross sections and terrestrial and space error rates for a range of circuits and environmental conditions. The level of simulation complexity increases when one must identify all sensitive nodes and their associated critical charges in larger circuits, and relate that information to an operational SEU rate. When SEUs occur as a result of multiple nodes being simultaneously affected by a single ion strike it has been shown that critical charges for multiple node processes are not discrete

Manuscript received July 11, 2008; revised September 08, 2008. Current version published December 31, 2008. This work was supported in part by the Defense Threat Reduction Agency, The Rad Hard Electronics for Space Exploration (RHESE) and in part by NASA Electronic Parts and Packaging (NEPP) program. The computational portion of this work was performed with the resources of Vanderbilt University's Advanced Computing Center for Research and Education (ACCRE).

K. M. Warren and A. L. Sternberg are with The Institute for Space and Defense Electronic, Vanderbilt University, Nashville, TN 37203 USA (e-mail: kevin.m.warren@vanderbilt.edu; andrew.l.sternberg@vanderbilt.edu).

R. A. Weller, L. W. Massengill, R. A. Reed, and R. D. Scrimpf are with the Electrical Engineering and Computer Science Department, Vanderbilt University, Nashville, TN 37235 (e-mail: robert.a.weller@vanderbilt.edu; lloyd.massengill@vanderbilt.edu; robert.reed@vanderbilt.edu; ron.schrimpf@vanderbilt.edu).

M. P. Baze is with the Boeing SSED, Seattle, WA 98124 USA (e-mail: mark.p.baze@boeing.com).

M. H. Mendenhall is with the Electrical Engineering and Computer Science Department and the Vanderbilt University Free Electron Laser Facility, Vanderbilt University, Nashville, TN 37235 USA (e-mail: marcus.h.mendenhall@vanderbilt.edu).

Digital Object Identifier 10.1109/TNS.2008.2006481

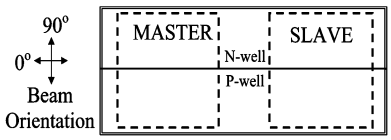

Fig. 1. Block level diagram of a single hardened flip-flop (right) and orientation marker (left). Note that the master and slave stages are physically separated. Each stage maintains a redundant data-path to increase SEU resistance.

values, but rather a continuum of values, resulting in a potentially infinite solution space of node combinations and critical charges [18]–[21]. Not all node combinations may be vulnerable and some may not be physically significant from a cross section or error rate perspective due to their physical spacing or location within the circuit. A full solution at the TCAD level in identifying all valid error conditions for larger circuits (containing 10 or more transistors) is not yet numerically feasible for evaluating SEU errors for a single ion, much less the full spectrum of ions required to provide an environmental characterization over space or terrestrial environments and the associated possible strike angles and positions.

II. Experiment

The circuit analyzed in this study is a radiation hardened, master-slave flip-flop containing 64 transistors, fabricated in a 90 nm CMOS technology. A block diagram of the flip-flop is shown in Fig. 1. SEU resistance is achieved through spatial redundancy of the data-path in each stage where a change in logic state occurs only if the states of the internal data-lines are in agreement [22]. The dimensions of the flip-flop are 31.4 μm and 3.82 μm along the zero degree and 90 degree axes, respectively. Flip-flops were placed on a test chip in single-file, shift register fashion. In addition, temporally coincident errors between shift register chains were identified in order to differentiate upsets due to transients in the external clock circuitry.

Heavy ion irradiation was performed at the Lawrence Berkeley National Laboratory. Ion species were Argon, Copper, Xenon, Neon, Oxygen, Boron, and Krypton with linear energy transfers (LETs) ranging from 3.45 to 62.6 $\mathrm{MeVcm^2/mg}$. Irradiations were performed at zero and at sixty-degree tilt angles. In addition, at sixty degrees of tilt, cross sections were recorded for orientations along the long axis of the part (zero degrees of roll) and perpendicular to the long axis (90 degrees of roll) as shown in Fig. 1.

III. Simulation

Simulations were performed using the Vanderbilt University Monte Carlo Radiative Energy Deposition software integrated with the Synopsys HSPICE circuit simulator. MRED was used for particle transport and energy deposition calculations and SPICE was used to evaluate the circuit level response to the particle events.

A. Particle Transport and Energy Deposition

MRED is based on Geant4 [1], which comprises physics models for the transport of radiation through matter. MRED also incorporates methods for parsing geometrical objects, such as solid models generated in computer aided design (CAD) software and can track energy deposition on an event-by-event basis in an unlimited number of regions within that solid model. The particle type (atomic number, mass, and energy), as well as the direction, is defined by the experimental or environmental conditions that are being simulated. The ion is transported through the solid model of the circuit, as in the master slave flip-flop evaluated in this paper, shown in Fig. 2. Energy loss can be modeled using both electronic and nuclear scattering processes.

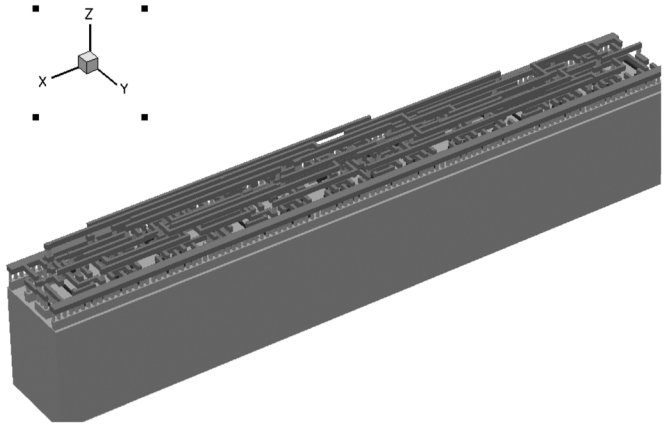

Fig. 2. Solid model representation of the flip-flop circuit showing metallization and polysilicon only. The structure simulated in MRED contained the full geometrical and material representation of the master-slave flip flop, including inter-layer dielectrics and passivation. Energy deposition was tracked in the sensitive volumes placed within the solid model.

B. Collected Charge

Energy deposition was monitored in the sensitive volume set for each transistor. Unlike the single-volume rectangular parrallel piped (RPP) approach commonly used for sensitive volume representation, the MRED tool allows one to represent the charge collection volume as a composite set of any arbitrary number of geometries, subsequently referred to as micro-volumes in this work. The user can define the overall number of possible micro-volume sets to represent a multitude of sensitive regions. In this application, it was convenient to describe a set for each transistor in the circuit shown in Fig. 2.

The dimensions of the sensitive volumes are largely determined by layout and processing features of the technology. For example, as shown in Fig. 3, the lateral and depth dimensions of $\mathrm{V_1}$ and $\mathrm{V_2}$ are the boundaries and depth of the active silicon regions adjacent to the shallow trench isolation (STI), respectively. The depth of $\mathrm{V_4}$, and to a lesser extent $\mathrm{V_3}$, is determined by the n/p-well and/or epitaxial junction depths. The final lateral dimensions and positioning of $\mathrm{V_3}$ and $\mathrm{V_4}$ are used as adjustable parameters in the calibration of the model to experimental data, discussed in a subsequent section.

The relationship between the deposited energy in the sensitive volume set for transistor i, from a single ionizing event and the charge collected at the transistor node is described by (1), where N is the total number of micro-volumes in the sensitive volume set representing the struck transistor. $\mathrm{E_{dep,j}}$ is the energy deposited by the event (see Fig. 3) and α_j is the charge collection efficiency of the jth micro-volume. The conversion

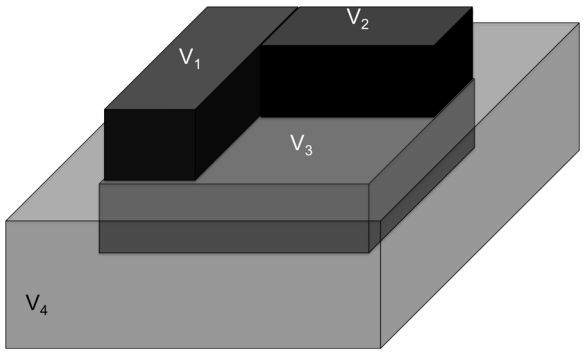

Fig. 3. A conceptual drawing of a micro-volume set for a single transistor. V1 and V2 are located within the active silicon region and V3 and V4 approximate charge collection from the substrate.

factor of 22.5 MeV/pC assumes that 3.6 eV are required, on average, to produce one electron-hole pair in silicon. In this study, only charge generated in the silicon is considered

$$Q_{col,i,j} = 22.5\ \frac{\text{MeV}}{\text{pC}} \sum_{j=1}^{N} \alpha_j E_{dep,j}. \tag{1}$$

The charge collection efficiency, α_j, is a free parameter associated with each micro-volume. It may be interpreted as the coefficient that relates the charge generated in a region enclosed by the micro-volume to the quantity of charge that is ultimately collected at the circuit node (transistor contact). For example, in Fig. 3, one may conclude that the efficiencies of V_1 and V_2 are much larger than that of the portion of region V_4 not containing V_3 due to a higher probability of recombination in areas far from the drain-body junctions.

C. The SPICE Interface

Following a particle event and a complete conversion of deposited energy to collected charge for each transistor in the circuit, the simulator queues the results into an event array. In this study, after 50 valid events were counted, the Monte-Carlo simulation (particle transport component) was halted and the collected charge queue automatically passed to the SPICE interface.

The SPICE interface is written in Python and manages the conversion of charge to double exponential current pulses, generates netlists with the appropriate current pulses, executes the SPICE simulator, and analyzes the resultant output for single event errors. A commercial version of HSPICE was used to analyze the circuit response.

It is important to recognize that each particle event could result in one, two, or many values of collected charge depending on the number of struck transistors. Thus, an *event* refers to the array of collected charge or charges, indexed by transistor name (the name provides a correlation between sensitive volume set and the netlist), to a single parent particle.

D. Current Pulse Calculation

The SPICE current pulse for a given Q_{coll}, is divided into three regions, each of which is described in (2), where t is time, t_{d1} is the pulse delay time, t_{d2} is the onset of the pulse decay, τ_1 is the rise time, τ_2 is the decay time, and I_m is the peak current. The integral of all current over time must be equal to the total collected charge (3) where I_1 and I_2 are the current in the rise and fall regions of the current pulse, respectively, and Q_1 and Q_2 refer to the charge collected in those regions.

For times less than the t_{d1}, the node current is zero. The current then rises and saturates from t_{d1} to t_{d2} (depositing Q_1) and decays from t_{d2} to infinite time (depositing Q_2). It is assumed that positive charge is deposited on all struck PMOS drain nodes and positive charge is removed from NMOS drain nodes

$$\begin{aligned} I_0(t) &= 0 \quad \{t < t_{d1}\} \\ I_1(t) &= I_m \left[1 - e^{-\frac{(t-t_{d1})}{\tau_1}}\right] \quad \{t_{d1} \le t < t_{d2}\} \\ I_2(t) &= I_m e^{-\frac{(t-t_{d2})}{\tau_2}} \quad \{t \ge t_{d2}\} \end{aligned} \tag{2}$$

$$Q_{coll} = \int_0^{\infty} I(t)dt = \int_{t_{d1}}^{t_{d2}} I_1(t)dt + \int_{t_{d2}}^{\infty} I_2(t)dt = Q_1 + Q_2. \tag{3}$$

In order to satisfy the conditions of (3) the parameters of (2) must be calculated for each Q_{coll}. Furthermore, it is assumed that the peak current, I_m, saturates at a value that is limited by the impedance of the struck node. Therefore, two possible cases exist during the calculation of the current pulse parameters:

Case 1) The simulator evaluates whether the collected charge is sufficient to saturate the current on the node (4)

$$\text{If}: \quad Q_{coll} < \frac{V_{DD}}{R_{on}} \left[(\tau_2 + \tau_1) + (t_{d2} - t_{d1}) - t_1 e^{-\frac{t_{d2}-t_{d1}}{\tau_1}}\right] \tag{4}$$

$$\text{Then}: \quad I_m = \frac{Q_{coll}}{(\tau_2 + \tau_1) + (t_{d2} - t_{d1}) - t_1 e^{-\frac{t_{d2}-t_{d1}}{\tau_1}}}. \tag{5}$$

For the analysis described here, V_{DD}, the supply voltage, is 0.9 V and the following assumptions are made: R_{on} the on-state resistance of the complementary device, is 1000 Ω, $\tau_1 = 2$ pS, $\tau_2 = 5$ pS, and $t_{d2} - t_{d1} = 10$ ps. Therefore, given the above parameters under the condition established in (4), the peak current, I_m, is calculated according to (5), which can be simplified to (6)

$$I_m(A) = 5.9 \times 10^{10} \cdot Q_{coll}(C) \quad if \quad Q_{coll} < 15.2\ \text{fC}. \tag{6}$$

Case 2) Given that the collected charge exceeds the condition in (4), a saturated current (7) is calculated

$$I_m = \frac{V_{DD}}{R_{on}} = 900\ \mu\text{A} \tag{7}$$

$$f = \frac{Q_1}{Q_{coll}} \equiv 0.67 \tag{8}$$

$$\tau_2 = (1-f)\frac{Q_{coll}}{I_m} \tag{9}$$

$$(t_{d2} - t_{d1}) - \left(\frac{Q_{coll}}{I_m}\right) + \tau_1 \left(e^{-\frac{(t_{d2}-t_{d1})}{\tau_1}} - 1\right) = 0. \tag{10}$$

τ_1 is 2 pS and f, the fraction of charge in the interval between t_{d1} and t_{d2}, is chosen to be 0.67 (8). This value was estimated

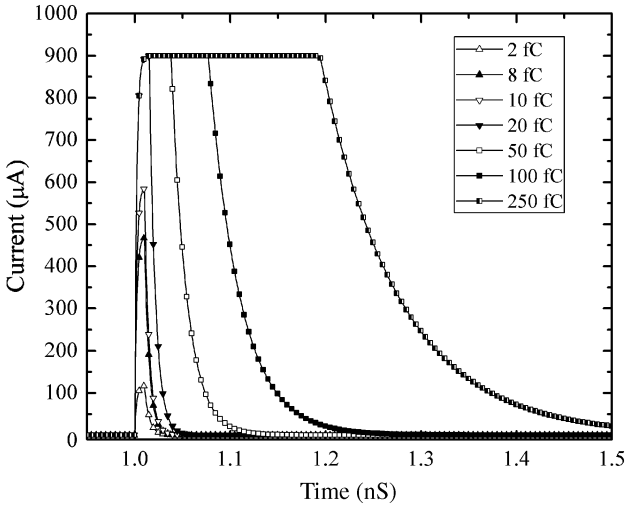

Fig. 4. Example double exponential current profiles over a range of Q_{coll}, the collected charge. Note that in this example, t_{d1}, the delay for the start of the current pulse, is 1 nS.

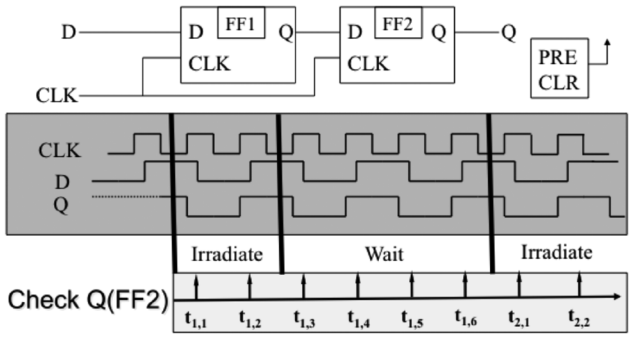

Fig. 5. Diagram of the current pulse injection and upset monitoring sequence of the flip-flop circuit. FF1 was irradiated and Q(FF2) was monitored to determine if an error originating in FF1 was latched. Q(FF2) was sampled at each CLK from [0, 6T].

from investigating TCAD simulations of similar technologies. The decay constant, τ_2, for Q_2 was calculated according to (9). Equation (10) was then solved for $t_{d2} - t_{d1}$.

A series of current pulses corresponding to collected charges from 2 fC to 250 fC is shown in Fig. 4. For $Q_{col} < 15$ fC, the peak current is less than the saturating current of 900 μA (Case 1) and increases with increasing Q_{coll}. As the collected charge continues to increase beyond 15 fC, the current pulse is stretched in such a manner as to satisfy (3) (Case 2). The double exponential current pulse is an approximation and is most justifiable for short pulse durations, (small values of collected charge). Long pulse durations at very large values of collected charge are likely unphysical, however, as will be shown in subsequent sections, small values of collected charge were found to dominate the calculated SEU rate.

E. Charge Injection Sequence and SEU Analysis

The SPICE interface automatically builds a netlist containing the calculated double exponential current sources from a template netlist. The template contains two identical flip-flops as shown in Fig. 5, but only accepts current pulses on nodes contained in FF1.

For each event, a t_{d1} (2) is randomly chosen between 0 and 2T, where T is the clock period. The t_{d1} is the same for all current pulses associated with a single *event*. That is, the *event* is assumed to occur at a random time between [0, 2T].

The output of the second flip-flop, FF2, is monitored for errors at Q. The second latch provides a means for differentiating transient errors in Q(FF1) from latched errors, recognizing that under dynamic conditions, transients in Q(FF1) may be latched into FF2. The FF2 is not modeled in radiation transport and exists only in SPICE as a means for detecting SEU in FF1.

For all simulations the clock frequency was 1 MHz and alternating logic levels were clocked into the data line of FF1, D(FF1), during simulation to ensure that all possible combinations of external signal levels and internal flip-flop states were evaluated. Four full clock periods beyond the maximum injection time were evaluated to ensure that any possible SEU had propagated to the FF2 output, Q(FF2).

F. Cross Section and Error Rate Calculation

The calculation of the per bit heavy ion SEU cross section (σ_{SEU}) in the simulation is performed in a manner identical to that of a heavy ion, broadbeam facility as described in (11)

$$\sigma_{SEU} = \frac{N}{F \cdot S}. \tag{11}$$

N is the number of counted errors for a given exposure, S is the number of bits irradiated, and F is the particle fluence of the exposure.

Unlike heavy ion facilities, where the fluence is provided, the simulator fluence is calculated according to (12) where i is the number of particle events and R_t is the randomization area of the particle beam

$$F = \frac{i}{R_t}. \tag{12}$$

The calculation of the error rate in a given radiation environment is discussed in [6] and a comprehensive description is beyond the scope of this paper. However, particle sampling is chosen from a given radiation environment provided to the simulator. The spatial aspect of the irradiation is randomized to simulate an isotropic environment, such as that experienced in space. The final rate is thus dependent on the area of the sphere encompassing the target object (flip-flop), the number of simulated events, and the scaling of the error count to particle flux. However, the calculation of the number of errors is performed in an identical manner for all simulated environments (experimental, terrestrial, or space).

G. Calibration

The output of the heavy ion broadbeam simulations is in the form of SEU cross section as a function of ion species. Consequently, the validity of the methodology, as well as the calibration of the adjustable parameter set associated with the simulation model, is tested against heavy ion broad-beam data.

The sensitive volume set and associated micro-volume parameters are varied in such a way as to visually minimize the difference between the simulation and experiment cross sections. Algorithms for automating this process are under consideration but have not yet been implemented. Currently, the best method of calibration to date is as follows:

1) Assign a sensitive volume with unity efficiency in the active regions of the transistors in the solid model. The volumes are located within the drain diffusion of each transistor.
2) Assign a sensitive volume of unity efficiency to each transistor, which extends into the substrate to a depth approximately equal to the n-well depth (CMOS).
3) Perform simulations and evaluate the results.
4) Add micro-volumes to volume sets in step 2 with less than unity efficiency, which generally extend deeper into the substrate and laterally outward from the volumes in (2). Sensitive volumes sets should be modified equally to reduce the parameter-space as well as to limit unintentionally biasing the sensitivity of a small set of transistors.
5) Adjust efficiencies to shift cross sections, from threshold or otherwise, to match data.
6) Repeat step #3.

Note that external results, such as those obtained through TCAD can be used to reduce the number of iterations. No parameters exceeded physically justifiable values. For example, the boundaries of the micro-volumes did not extend into SiO_2 and their depths were approximately equal to known junction depths. For the simulations described in this work, a maximum efficiency of 100% was used for the drain node region of the NMOS devices with a maximum collection depth of 1.5 μm at an efficiency of 5%. Likewise, the drain regions of the PMOS devices were limited to 70% collection efficiency and the maximum collection depth was 0.80 μm with an efficiency of 2%.

IV. Results

A. Heavy Ion Calibration

The cross section curve for the experimental and simulated broadbeam experiment at normal incidence is shown in Fig. 6. Good agreement was achieved by extending lateral dimensions of the sensitive volumes to allow for overlap. In this manner, charge sharing between devices was factored into the simulation. This mechanism has previously been shown to play a role in soft errors for this technology [20].

Greater deviation is seen at the 60 degree tilt and 0 degree roll condition as shown in Fig. 7. Although the saturation cross sections differ, the most likely impact on the calculated soft error rate is the apparent difference in threshold LET. Fig. 8 contains the heavy ion data for irradiation at 90 degrees of roll and 60 degrees of tilt. The simulation model over-predicts the cross sections under these conditions. This is the only irradiation for which errors were shown in either simulation or experiment to occur below an LET of 10 $\mathrm{MeVcm^2/mg}$. The *Analysis* section of this paper discusses the impact of errors in calibration on the calculated soft error rate.

The extent to which the sensitive volume dataset for this flip-flop could be calibrated was limited by the existence of three unique irradiation angles. Thus, a priority was placed on capturing the trend of the cross section data in the calibration stage. Extensive adjustment of the sensitive volume sets' parameters could not be justified without further experimental results. However, the good qualitative (trend) agreement as well as qualitative agreement at the largest values of SEU cross section was deemed adequate for analyzing the flip-flop's SEU mechanisms and predicting the on-orbit SEU rate.

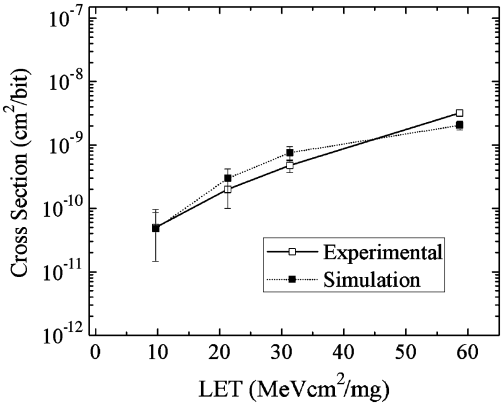

Fig. 6. Experimental and simulated cross sections at normal incidence for the latch. No errors were found to occur below 10 $\mathrm{MeVcm^2/mg}$ in either simulation or experiment.

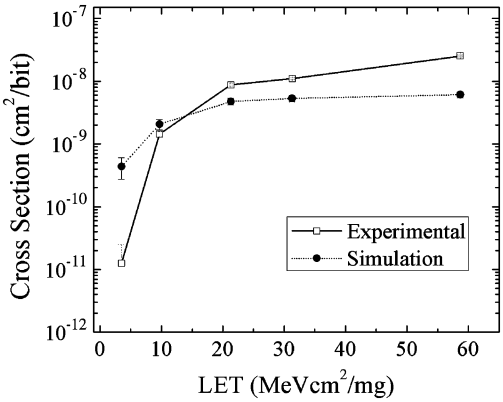

Fig. 7. Simulated and experimental cross sections at 60° tilt, 0° roll.

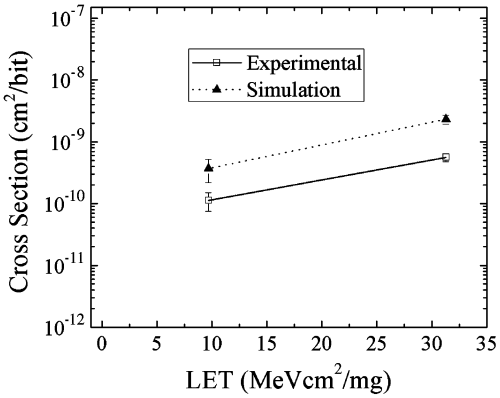

Fig. 8. Heavy ion cross sections at 60 degree tilt, 90 degree roll angles. No errors were measured or shown to occur in simulation below 10 $\mathrm{MeVcm^2/mg}$.

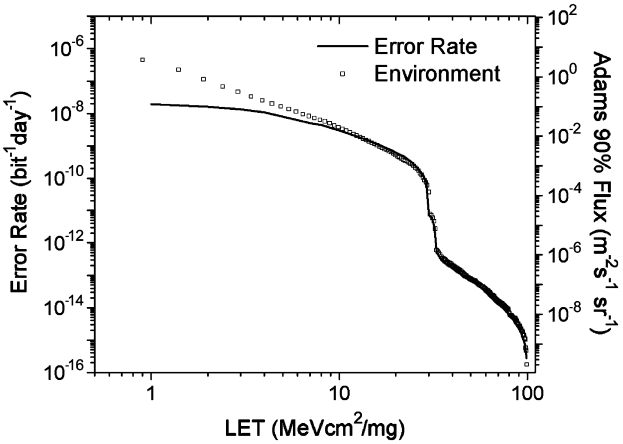

Fig. 9. The integral LET spectrum for the Adams 90% environment (open squares) and the equivalent response plot of the DICE latch (solid line).

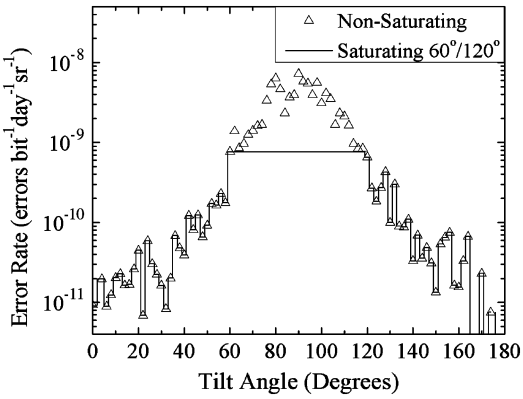

Fig. 10. Solid-angle normalized error rate as a function of the ions' tilt component from the on-orbit SEU rate calculation (open triangles) integrated over all roll angles. The solid line represents a saturation of the error rate beyond 60°.

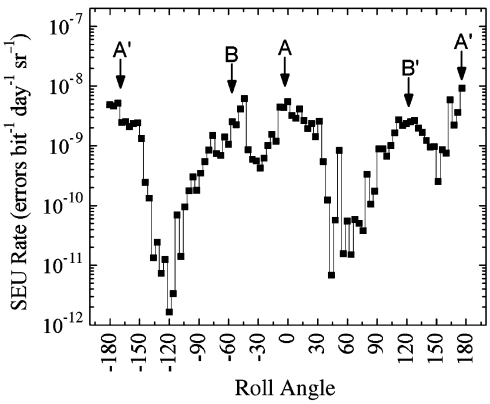

Fig. 11. Solid-angle normalized error rate as a function of the ions roll component of the directional vector from the on-orbit SEU rate calculation integrated over all tilt angles.

B. SEU Error Rate

The ultimate application of the coupled MRED and SPICE simulators is the prediction of error rates. Specifically, for this study the objective is to determine the on-orbit error rate under the Adams 90% worst-case conditions. Although highly conservative in its heavy ion flux levels, the environment is considered appropriate for some programs in which an absolute upper-bound on the on-orbit SER is required.

Fig. 9 contains the integral LET spectrum for all species from $Z = 1$ (H) to $Z = 92$ (U). Although MRED does not calculate charge generation by path lengths and stopping power tables, the integral LET spectrum provides a useful representation of the environment. In performing the transport simulations, MRED samples from the differential flux spectra associated with the environment. The spectrum of each atomic species is passed to MRED, from $Z = 1$ to $Z = 92$, and the absolute contribution of each species to the on-orbit SEU rate is determined.

The simulator uses an identical parameter set to that of the heavy ion broadbeam simulations, but the type of events are changed from single particle species to a sampled spectrum and the particles are directed at the flip-flop model isotropically.

Computational requirements were 2400 CPU-hours distributed over 100 processors on the Vanderbilt Advanced Computing Center for Research and Education (ACCRE) computing cluster [23]. The calculation required 1.0×10^8 simulated particle events, resulting in over 12500 SPICE simulations. The simulation predicted a final calculated SEU rate of $1.9 + / - 0.1 \times 10^{-8}$ e/b/d. The uncertainty in the estimate is a single standard deviation and incorporates the counting error associated with Monte-Carlo simulation. It is not a reflection of the systematic uncertainty in the method.

A comparison between the flux of particles as a function of LET and the contribution of those particles to the SEU rate is illustrated in Fig. 9. Above 10 $\mathrm{MeVcm^2/mg}$ the integral flux and integral error rate track by a uniform scale factor. The divergence of the two curves below 10 $\mathrm{MeVcm^2/mg}$ illustrates the decreased probability of low LET particles contributing to the SEU rate. The simulator reports an increase in the SEU rate to approximately 2 $\mathrm{MeVcm^2/mg}$, which can be viewed as an omni-directional threshold LET. This value is below that measured under the limited experimental broadbeam conditions. The effect of the omni-directional threshold LET on the calculated SEU rate is discussed in greater detail in the *Sources of Uncertainty* section of the paper.

The directional vectors of the heavy ions that resulted in SEUs were tracked and are plotted in Fig. 10 and Fig. 11 as a function of their contribution to the SEU rate. The scatter associated with Figs. 10, 11 is due to both simple counting error and the weighting scheme used in spectral sampling [17]. In Fig. 10, the open triangles represent the simulator output as a function of tilt angle and indicates that a substantial portion of the predicted errors occur outside of the range of calibration (between 60 and 120 degrees). The solid line is discussed in the *Sources of Uncertainty* section of the paper. Fig. 11 indicates peaking for two distinct directions, labeled A and B in the figure. The circuit level cause of the peaks is discussed in the *Circuit Level Effects* subsection of the *Analysis* section. As in Fig. 10, a significant portion of the overall SEU rate is predicted to occur outside of the region of heavy ion calibration.

V. Analysis

Previous work has demonstrated the ability to use the multiple sensitive volume model in MRED to reproduce SEU cross sections accurately in radiation hardened latches [11]. In [11],

TABLE I
THE ERROR RATE FOR THREE TYPES OF MULTI-NODE EVENTS

Event Type	Error Rate (e/b/d)
All Events	1.9 +/- 0.1 x 10^{-8}
NMOS only	4.8 +/- 0.8 x10^{-9}
PMOS only	4.5 +/- 0.4 x10^{-9}
N and PMOS	1.1 +/- 0.1 x10^{-8}

extensive data sets over a large range of roll and tilt angles allowed for a detailed analysis of the interaction between sensitive volume sets and consequently good quantitative agreement with experimental data was achieved. Unlike [11], the analysis technique presented in this work incorporates SPICE, which eliminates *a priori* knowledge about the SEU mechanisms, sensitive nodes, and critical charges of the circuit under investigation. SPICE analysis on an event-by-event basis provides a mean to investigating, validating, and improving single event upset performance.

A. Circuit Level Effects

Identifying the cause of SEU in the particular circuit under consideration is critical for the purpose of improving subsequent layout and circuit design and is a substantial advantage of the method presented in this work over other techniques. As MRED tracks all information related to each event, it is possible to analyze the contribution of any transistor or combination of transistors to the final SEU cross section or SEU error rate. With the inclusion of SPICE, the simulation inherently provides a layout-to-schematic correlation useful for investigating the mechanisms of SEU.

As an example, post-processing of simulation data was performed to identify errors that resulted from coupling, either by coincidence or charge sharing, between NMOS devices, PMOS devices, and those events that resulted from coincident charge deposition in NMOS and PMOS transistors. The contribution of each type is contained in Table I. The overall error rate is shown to be almost equally dependant on mixed transistor type events (labeled *N and PMOS*) and those from NMOS and PMOS only.

An excerpt of the flip-flop layout is shown in Fig. 12 with the circuit schematic of the master stage. The transistors shown in the layout are NMOS devices and the type of event is considered here as *NMOS only*. These types of events are found in the A and A' peaks of Fig. 11. For this specific event, the ion passed through two sets of NMOS transistors (labeled 26–27, 30–32). By inspection of the circuit schematic, it is clear that each set drives a different redundant data path and both N1 and N2 are simultaneously pulled low, causing the master stage to upset during clock-high conditions. Similar effects were observed over the entire device as illustrated in Fig. 13. The frequency of events, as reflected in the SEU rate calculation, is due to the physical proximity of the nodes. An increase in separation of the devices will result in a decrease in the predicted SEU rate from this type of event. Although coincidence charge collection is possible for certain ion trajectories, an increase in spacing will reduce or eliminate charge sharing [20] and cause a decrease in the SEU rate.

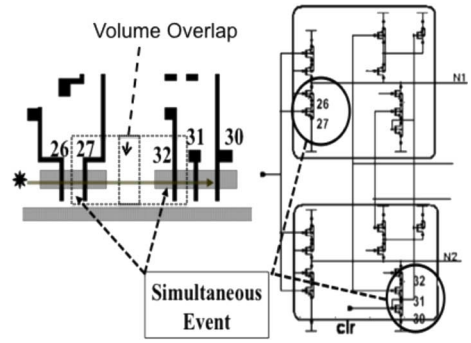

Fig. 12. Schematic and layout views illustrating charge sharing between NMOS devices. The sensitive volume overlap resulted in errors at normal incidence with cross sections that increased with increasing tilt angle.

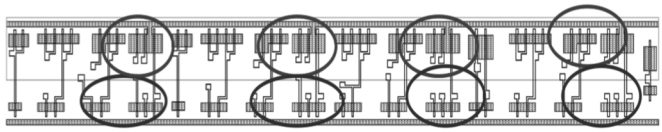

Fig. 13. Layout view of the master—slave flip flop with the SEU sensitive regions circled. The events limited to one type of device (e.g. all NMOS) were concentrated in these regions and represent a layout driven vulnerability identified by circuit analysis.

B. Sources of Uncertainty—Systematic Error

The nature of Monte-Carlo simulations as well as the circuit level response prediction by SPICE results in a single event error rate that is achieved via a non-analytical solution. Consequently, the SEU rate cannot be described as a function of the sensitive volume (and other) parameters, and a systematic uncertainty in the method itself as a function of these parameters is not readily attainable.

As has been shown in previous sections, MRED simulations provide a comprehensive set of information pertinent to the analysis of each radiation evident. For example, the stopping power of ions can be calculated during run-time and logged. By inspection of Fig. 7, the calibrated MRED model the cross section at an LET of 3.5 $\mathrm{MeVcm^2/mg}$ and subsequently is under-estimating the threshold LET. In Fig. 9, the cumulative error rate contribution as a function of LET is shown against the environment. By rejecting events that occur below a given LET, the impact of inaccuracies of the model in predicting threshold LET (or the experimental data in improperly quantifying it) can be evaluated. Table II contains the error rate for rejection of events for a hypothetical cutoff in LET of 5.0 and 9.5 $\mathrm{MeVcm^2/mg}$, which results in a calculated error rate of $8.0 + / - 0.3 \times 10^{-9}$ and $3.2 + / - 0.1 \times 10^{-9}$ $\mathrm{e/b/d}$, respectively. From the perspective of sensitive volume parameterization, the logical deduction is that the efficiency of a small volume or set of volumes is too high, or that for a given efficiency, their dimensions are too great. A rigorous treatment of impact of sensitive volume parameterization on the error rate would require slightly varying each parameter, would be unique to each simulation, and demand extremely long computational times using current hardware.

Experimental limitations, generally in the form of a sufficient number of roll and tilt angles to quantify a device's cross sec-

TABLE II
THE BASELINE SEU RATE AND THE EFFECT OF LIMITING THE OMNIDIRECTIONAL LET ($\mathrm{LET}_{\mathrm{CUTOFF}}$), THE SEU RATE AT STEEP TILT ANGLES, AND THE COMBINATION OF FACTORS ON THE CALCULATED SEU RATE

Condition	SEU Rate (e/b/d)
No Limits, Full Simulation	1.9 +/- 0.1x 10^{-8}
$\mathrm{LET}_{\mathrm{cutoff}}$ = 5.0	8.0+/- 0.3 x 10^{-9}
$\mathrm{LET}_{\mathrm{cutoff}}$ = 9.5	3.2 +/- 0.1 x 10^{-9}
60° tilt saturation	5.7+/- 0.4 x 10^{-9}
$\mathrm{LET}_{\mathrm{cutoff}}$ = 5.0 / 60° tilt	3.5+/- 0.2 x 10^{-9}
$\mathrm{LET}_{\mathrm{cutoff}}$ = 9.5 / 60° tilt	1.2 +/- 0.2 x 10^{-9}

tion completely, may also play a role in uncertainty in the calculated SEU rate. For example, the SEU rate over tilt angles shown in Fig. 10 continues to increase beyond 60 degrees and peaks at grazing incidence, beyond the angle for which experimental cross sections were measured. The solid line in Fig. 10 represents an artificial limitation on the SEU rate in which its value is forced to saturate at the 60° tilt value. Under these conditions, the SEU rate was calculated to be $5.7 + / - 0.4 \times 10^{-9}$ e/b/d, a reduction of approximately 3.5 fold in the baseline SEU rate. Similarly, the off-axis peaking in the roll angle response shown in Fig. 11 as peaks B and B′ indicates a strong SEU response outside the range of data. Unlike grazing incidence SEU cross section measurements, which are difficult to make due to ion range limitations at most test facilities, the off-axis roll rate warrants a broader heavy ion test and dataset to refine the SEU rate prediction.

VI. CONCLUSIONS

By incorporating both radiation transport and SPICE simulation tools into a single automated simulation flow it is possible to identify single event upset vulnerabilities from both a layout and circuit perspective with no user intervention during run time. The method described in this work utilizes a SEU model based on the physics of energy deposition, the charge collection at each transistor, and the circuit response to the collected charge or charges. The model is physically based and incorporates descriptions of the radiation environment, as well as experimentally-determined device response. The results are useful for guiding subsequent re-designs and identifying the effects of layout modifications on the SEU cross sections and SEU rate, as they directly relate the layout to the circuit performance. Furthermore, the simulations can be used to verify that the heavy ion test campaign used to calibrate the models was adequate for predicting SEU error rates accurately.

The flexibility of the MRED interface allows one to investigate the effects of potential errors in the model's calibration with respect to the SEU rate in the isotropic environment (e.g. Adams 90%). For example, in the specific case considered here, the imposition of an $\mathrm{LET}_{\mathrm{cutoff}}$ of 5.0 $\mathrm{MeVcm}^2/\mathrm{mg}$ in the SEU rate calculation reduces the predicted rate to $8.0 + / - 0.3 \times 10^{-9}$ e/b/d, where the error represents one standard deviation from the counting statistics inherent to Monte-Carlo simulation. This limitation is justifiable in light of the over-prediction of cross section at low LET from the heavy ion experimental data-set with respect to the simulator prediction, and indicates a large degree of sensitivity to the threshold LET in the model.

The treatment of systematic uncertainty was also extended to include limitations in the experimental dataset. The isotropic (on-orbit) simulation results show that the largest contribution to the on-orbit SEU rate is particles arriving at grazing incidence (large tilt angles), beyond the range of experimentally available data (60°). Imposing a saturating value at 60° of tilt on the environmental prediction reduces the SEU rate to $5.7 + / - 0.4 \times 10^{-9}$ e/b/d, 3.5 times lower than the value obtained without considering saturation.

Coincident charge collection between NMOS and PMOS transistors was observed to produce upsets (B and B′ peaks of Fig. 11) for off-axis directions. SEUs of this type contribute approximately as much to the overall SEU rate as events involving multiple nodes of the same polarity; therefore only separating NMOS or PMOS devices is not sufficient alone to reduce the SEU rate beyond a factor of 2 in this circuit. Although errors were measured at 90° of roll, the simulation results suggest that further heavy ion testing is required for more roll angle conditions to quantify the SEU cross section accurately.

An SEU error rate of $1.9 + / - 0.1 \times 10^{-8}$ e/b/d was calculated for the hardened flip-flop presented in this work. A comprehensive analysis of potential systematic error from the calibrated model suggests that the SEU rate may vary from this value by as much as an order of magnitude. It is important to recognize that this level of fidelity is not a function of the methodology, but is a function of the limitations in experimental data and model calibration error. If design requirements are such that the error rate must fall outside of the range presented here, a redesign of the circuit or is warranted.

To reduce the overall rate, redesign of the integrated circuit is required to eliminate charge sharing between proximate NMOS devices, proximate PMOS devices, as well as the coincident charge collection between NMOS and PMOS transistors. An adequate range of tilt and roll angle heavy ion irradiations must be part of test plans when measuring SEU cross sections in single-node hardened circuitry to calibrate models accurately and predict on-orbit SEU rates, as well as identify all possible coupling mechanisms.

REFERENCES

[1] S. Agostinelli, J. Allison, K. Amako, J. Apostolakis, H. Araujo, P. Arce, M. Asai, D. Axen, S. Banerjee, G. Barrand, F. Behner, L. Bellagamba, J. Boudreau, L. Broglia, A. Brunengo, H. Burkhardt, S. Chauvie, J. Chuma, R. Chytracek, G. Cooperman, G. Cosmo, P. Degtyarenko, A. Dell'Acqua, G. Depaola, D. Dietrich, R. Enami, A. Feliciello, C. Ferguson, H. Fesefeldt, G. Folger, F. Foppiano, A. Forti, S. Garelli, S. Giani, R. Giannitrapani, D. Gibin, J. J. Gomez, Cadenas, I. Gonzalez, G. Gracia Abril, G. Greeniaus, W. Greiner, V. Grichine, A. Grossheim, S. Guatelli, P. Gumplinger, R. Hamatsu, K. Hashimoto, H. Hasui, A. Heikkinen, A. Howard, V. Ivanchenko, A. Johnson, F. W. Jones, J. Kallenbach, N. Kanaya, M. Kawabata, Y. Kawabata, M. Kawaguti, S. Kelner, P. Kent, A. Kimura, T. Kodama, R. Kokoulin, M. Kossov, H. Kurashige, E. Lamanna, T. Lampen, V. Lara, V. Lefebure, F. Lei, M. Liendl, W. Lockman, F. Longo, S. Magni, M. Maire, E. Medernach, K. Minamimoto, P. Mora de Freitas, Y. Morita, K. Murakami, M. Nagamatu, R. Nartallo, P. Nieminen, T. Nishimura, K. Ohtsubo, M. Okamura, S. O'Neale, Y. Oohata, K. Paech, J. Perl, A. Pfeiffer, M. G. Pia,

F. Ranjard, A. Rybin, S. Sadilov, E. Di Salvo, G. Santin, T. Sasaki, N. Savvas, Y. Sawada, S. Scherer, S. Sei, V. Sirotenko, D. Smith, N. Starkov, H. Stoecker, J. Sulkimo, M. Takahata, S. Tanaka, E. Tcherniaev, E. Safai Tehrani, M. Tropeano, P. Truscott, H. Uno, L. Urban, P. Urban, M. Verderi, A. Walkden, W. Wander, H. Weber, J. P. Wellisch, T. Wenaus, D. C. Williams, D. Wright, T. Yamada, H. Yoshida, and D. Zschiesche, "Geant4-a simulation toolkit," *Nuc. Instr. and Methods A*, vol. 506, p. 250, 2003.

[2] C. Inguimbert, S. Duzellier, and R. Ecoffet, "Contribution of GEANT4 to the determination of sensitive volumes in case of high-integrated RAMs," *IEEE Trans. Nucl. Sci.*, vol. 49, no. 3, pp. 1480–1485, Jun. 2002.

[3] P. Truscott, F. Lei, C. S. Dyer, A. Frydland, S. Clucas, B. Trousse, K. Hunter, C. Comber, A. Chugg, and M. Moutrie, "Assessment of neutron- and proton-induced nuclear interaction and ionization models in Geant4 for simulating single event effects," *IEEE Trans. Nucl. Sci.*, vol. 51, no. 6, pp. 3369–3374, Dec. 2004.

[4] G. Gasiot, V. Ferlet-Cavrois, J. Baggio, P. Roche, and P. Flatresse, "SEU sensitivity of bulk and SOI technologies to 14-MeV neutrons," *IEEE Trans. Nucl. Sci.*, vol. 49, no. 6, pp. 3032–3037, Dec. 2002.

[5] K. M. Warren, R. A. Weller, R. A. , M. H. Mendenhall, R. A. Reed, D. R. Ball, C. L. Howe, B. D. Olson, M. L. Alles, L. W. Massengill, R. D. Schrimpf, N. F. Haddad, S. E. Doyle, D. McMorrow, J. S. Melinger, and W. T. Lotshaw, "The contribution of nuclear reactions to heavy ion single event upset cross-section measurements in a high-density SEU hardened SRAM," *IEEE Trans. Nucl. Sci.*, vol. 52, pp. 2125–2131, Dec. 2005.

[6] R. A. Reed, R. A. Weller, R. D. Schrimpf, M. H. Mendenhall, K. M. Warren, and L. W. Massengill, "Implications of nuclear reactions for single event effects test methods and analysis," *IEEE Trans. Nucl. Sci.*, vol. 53, no. 6, pp. 3356–3362, Dec. 2006.

[7] K. M. Warren, B. D. Sierawski, R. A. Weller, R. A. Reed, M. H. Mendenhall, J. A. Pellish, R. D. Schrimpf, L. W. Masengill, M. E. Porter, and J. W. Wilkinson, "Predicting thermal neutron-induced soft errors in static memories using TCAD and physics-based Monte Carlo simulation tools," *Elect. Dev. Lett.*, vol. 28, no. 2, pp. 180–182, Feb. 2007.

[8] A. D. Tipton, J. A. Pellish, R. A. Reed, R. D. Schrimpf, R. A. Weller, M. H. Mendenhall, A. K. Sutton, R. Diestelhorst, G. Espinel, J. D. Cressler, P. W. Marshall, and G. Vizkelethy, "Multiple-bit upset in 130 nm CMOS technology," *IEEE Trans. Nucl. Sci.*, vol. 53, no. 6, pp. 3259–3264, Dec. 2006.

[9] K. M. Warren, R. A. Weller, B. Sierawski, R. A. Reed, M. H. Mendenhall, R. D. Schrimpf, L. W. Massengill, M. Porter, J. Wilkinson, K. A. LaBel, and J. Adams, "Application of RADSAFE to model single event upset response of a 0.25 micron CMOS SRAM," *IEEE Trans. Nucl. Sci.*, vol. 54, no. 4, pp. 898–903, Aug. 2007.

[10] A. S. Kobayashi, D. R. Ball, K. M. Warren, R. A. Reed, M. H. Mendenhall, R. D. Schrimpf, and R. A. Weller, "The effect of metallization layers on single event susceptibility," *IEEE Trans. Nucl. Sci.*, vol. 52, no. 6, pp. 2189–2193, Dec. 2005.

[11] K. M. Warren, B. D. Sierawski, R. A. Reed, R. A. Weller, C. Carmichael, A. Lesea, M. H. Mendenhall, P. E. Dodd, R. D. Schrimpf, L. W. Massengill, T. Hoang, H. Wan, J. L. Jong, R. Padovani, and J. Fabula, "Monte-Carlo based on-orbit single event upset rate prediction for a radiation hardened by design latch," *IEEE Trans. Nucl. Sci.*, vol. 54, no. 6, pp. 2419–2425, Dec. 2007.

[12] D. R. Ball, K. M. Warren, R. A. Weller, R. A. Reed, A. Kobayashi, J. A. Pellish, M. H. Mendenhall, C. L. Howe, L. W. Massengill, R. D. Schrimpf, and N. F. Haddad, "Simulating nuclear events in a TCAD model of a high-density SEU hardened SRAM technology," *IEEE Trans. Nucl. Sci.*, vol. 53, no. 4, pp. 1794–1798, Aug. 2006.

[13] [Online]. Available: http://www.reat.space.qinetiq.com/gemat/

[14] "Soft errors in circuits and systems," *IBM J. Res. Devel.*, vol. 52, no. 3, 2008.

[15] M. Turowski, A. Fedoseyev, A. Raman, K. M. Warren, and M. L. Alles, "Mixed-mode modeling of radiation effects with nuclear reactions in nanoscale electronics," in *Proc. 2008 GOMAC Conf.*

[16] C. Inguimbert and S. Duzellier, "SEU rate calculation with GEANT4 (comparison with CREME 86)," *IEEE Trans. Nucl. Sci.*, vol. 51, no. 5, pp. 2805–2810, Oct. 2004.

[17] R. A. Reed, R. A. Weller, M. H. Mendenhall, J.-M. Lauenstein, K. M. Warren, J. A. Pellish, R. D. Schrimpf, B. D. Sierawski, L. W. Massengill, P. E. Dodd, M. R. Shaneyfelt, J. A. Felix, J. R. Schwank, N. F. Haddad, R. K. Lawrence, J. H. Bowman, and R. Conde, "Impact of ion energy and species on single event effects analysis," *IEEE Trans. Nucl. Sci.*, vol. 54, no. 6, pp. 2312–2321, Dec. 2007.

[18] J. D. Black, A. L. Sternberg, M. L. Alles, A. F. Witulski, B. L. Bhuva, L. W. Massengill, J. M. Benedetto, M. P. Baze, J. L. Wert, and M. G. Hubert, "HBD layout isolation techniques for multiple node charge collection mitigation," *IEEE Trans. Nucl. Sci.*, vol. 52, no. 6, pp. 2536–2541, Dec. 2005.

[19] B. D. Olson, D. R. Ball, K. M. Warren, L. W. Massengill, N. F. Haddad, S. E. Doyle, and D. McMorrow, "Simultaneous single event charge sharing and parasitic bipolar conduction in a highly-scaled SRAM design," *IEEE Trans. Nuc. Sci.*, vol. 52, no. 6, pp. 2132–2136, Dec. 2005.

[20] O. A. Amusan, L. W. Massengill, M. P. Baze, B. L. Bhuva, A. F. Witulski, S. Dasgupta, A. L. Sternberg, P. R. Fleming, C. C. Heath, and M. L. Alles, "Directional sensitivity of single event upsets in 90 nm CMOS due to charge sharing," *IEEE Trans. Nucl. Sci.*, vol. 54, no. 6, pp. 2584–2589, Dec. 2007.

[21] R. Velazco, T. Calin, M. Nicolaidis, S. C. Moss, S. D. LaLumonDiere, V. T. Tran, and R. Koga, "SEU-hardened storage cell validation using a pulsed laser," *IEEE Trans. Nucl. Sci.*, vol. 43, no. 6, pp. 2843–2848, Dec. 1996.

[22] M. P. Baze, J. C. Killens, R. A. Paup, and W. P. Snapp, "SEU hardening techniques for retargetable, scalable, sub-micron digital circuits and libraries," in *21th SEE Symp.*, Manhattan Beach, CA, Apr. 2002.

[23] [Online]. Available: http://www.accre.vanderbilt.edu